Recent Experiments at the JPL Optical Communications Telescope Laboratory

Keith Wilson,* Joseph Kovalik,* Abhijit Biswas,* and William T. Roberts*

The JPL Optical Communications Telescope Laboratory (OCTL) facility is designed to investigate laser beam propagation strategies to support optical communications to NASA's deep-space probes. The OCTL has recently propagated 30-μrad beams to retroreflecting low-Earth-orbiting (LEO) satellites. This article describes these experiments and future experiment plans.

I. Introduction

Ground-to-space, space-to-space, and space-to-ground optical communications demonstrations have addressed critical issues such as space-to-space, space-to-ground acquisition pointing and tracking, and scintillation mitigation on ground-to-space links. [1–6]. The JPL Optical Communications Telescope Laboratory (OCTL) (Figure 1) is a state-of-the-art optical ground station located at a 2.2-km altitude in the San Gabriel Mountains of Southern Cali-

Figure 1. The OCTL facility at Table Mountain houses a 1-m azimuth/elevation coudé focus telescope.

*Communications Architectures and Research Section.

The research described in this publication was carried out by the Jet Propulsion Laboratory, California Institute of Technology, under a contract with the National Aeronautics and Space Administration.

fornia. It is designed for field demonstrations and research into strategies to mitigate the effects of the atmosphere on the deep-space optical link.

Located at longitude 117°40.9' W and a midlatitude of 34°22.9' N, OCTL can track satellites in low-Earth orbit (LEO) and geostationary and Molniya orbits. The facility houses an elevation/azimuth 1-m telescope (λ/7 RMS wavefront error at 632 nm) with a four-port coudé focus [7]. Designed to track 250-km-high LEO spacecraft with a 6-deg keyhole, the telescope slews at 10 deg/sec in elevation and 20 deg/sec in azimuth. All seven mirrors have protected silver mirror coatings and will support propagation of high-power laser beams over the wavelength band of 500 to 2200 nm. The telescope supports daytime and nighttime operations and has Sun-avoidance software built into its operation that allows it to point as close as 10 deg to the Sun. Specially designed shields protect the secondary mirror-support spiders from heating by off-axis solar reflection focused by the primary mirror. Recent experiments at the OCTL range from satellite imaging and active satellite tracking to adaptive optics correction of atmosphere-induced turbulence. This article reports the latest active satellite-tracking experiments that were conducted to validate the OCTL pointing and tracking capability.

II. Active Satellite Tracking Theory

The return signal from a retroreflector-bearing satellite can be estimated using the radar link below; the variables are defined in Table 1.

$$S = E_p\left(\frac{\lambda}{hc}\right)\eta_{TX}\,G_T\,L_P\,L_S\,\sigma_{BS}\,\eta_{atm}^2\,L_{atm\_Spread}\,L_{atm\_point}\,A\,\eta_{Rx\_Tel}\,\eta_{Strehl}\,\eta_{opt\_train}\,\eta_{POL} \tag{1}$$

Table 1. Terms in Equation (1).

Symbol	Parameter	Units
S	Signal photons incident on receiving detector	photons/pulse
h	Planck's constant	joule-sec
λ	Laser wavelength	m
c	Velocity of light	m/sec
E_p	Laser energy per pulse	joules
η_{TX}	Transmission efficiency	—
G_T	Transmitter gain	—
L_P	Pointing loss	—
L_S	Round-trip space loss	m^{-4}
σ_{BS}	Satellite backscattering cross-section	m^2
η_{atm}	Atmospheric transmittance	—
L_{atm_Spread}	Atmospheric spreading loss	—
L_{atm_point}	Atmospheric pointing loss	—
A	Telescope collection area	m^2
η_{Rx_Tel}	Receive telescope efficiency	—
η_{Strehl}	Loss due to wavefront error	—
η_{opt_train}	Receive optical train loss	—
η_{POL}	Receive polarization incompatibility loss	—

Laser Energy. The energy per pulse, E_p, of the laser is a measured quantity. The 532-nm output is approximately 65 mJ per pulse and the output at 1064 nm is 300 mJ.

Transmission Loss. The transmission efficiency, η_{TX}, is the product of (1) the optical throughput at the laser wavelength for the optical train that couples the laser output to the OCTL telescope coudé fold mirror (M7), and (2) the OCTL telescope transmission resulting from the reflection losses of the seven telescope mirrors and transmission loss through the path isolation window. An optical Strehl term is included in the transmission losses through the telescope. The Strehl loss is calculated assuming a 0.1 wave RMS wavefront error (WFE) at 633 nm. Thus, the WFE is scaled by wavelength and the Strehl is given by $\left[1-(2\pi\sigma_{WFE})^2\right]$. At 1064 nm, this loss is approximately 4 dB, whereas at 532 nm the loss increases to 6 dB.

Transmitter Gain. The on-axis transmitter gain, G_T, assumed for a quasi-Gaussian spatial profile is given by $8/\theta_t^2$, where θ_t is the half-angle between the beam center and the $1/e^2$ intensity point of the far-field divergence pattern.

Pointing Loss. The pointing loss, L_P, is calculated from fixed and random pointing losses for each axis of the OCTL telescope. The expression derived in [8] was used and is given by Equation 2:

$$L_P = \frac{\sigma'_{El}+\sigma'_{Az}}{\sigma_{El}\,\sigma_{Az}}\exp\left\{-2\left(\frac{\theta_{El}^2+\theta_{Az}^2}{\theta_t^2}\right)\right\}\exp\left\{\frac{2}{\theta_t^4}\left(\theta_{El}^2\sigma'^2_{El}+\theta_{Az}^2\sigma'^2_{Az}\right)\right\} \tag{2}$$

where $\sigma_{El(Az)}$ is the random pointing error in the elevation and azimuth axis and $\theta_{El(Az)}$ is the fixed pointing error in elevation and azimuth axes. Moreover,

$$\frac{1}{\sigma'^2_{El(Az)}} = \frac{1}{\sigma^2_{El(Az)}} + \frac{1}{\theta_t^2} \tag{3}$$

Space Loss. The round-trip space-loss term, L_S, is given by $(1/4\pi R^2)^2$.

Satellite Backscattering Cross-Section. Reference [9] gives a listing of the satellites, their altitudes, and backscattering cross-sections. Table 2 lists these quantities for the satellites illuminated in the active satellite tracking experiments.

Equation (4) gives the correction term for non-normal incidence [9]:

Table 2. Altitude and laser cross-sections of target satellites.

Spacecraft	Height, km	Backscattering Cross-Section, m^2
Beacon-C	940	3.6E+6
Stella	950	6.5E+5
Starlette	90	6.5E+5
EGP-1	1400	1.20E+7
LAGEOS	5900	7.00E+6

$$\eta(\theta_{inc}) = \frac{2}{\pi}\left(\sin^{-1}\mu - \sqrt{2\mu}\tan\theta_{ref}\right)\cos\theta_{inc} \tag{4}$$

where θ_{inc} is the angle of incidence and θ_{ref} is the internal refracted angle given by

$$\theta_{ref} = \sin^{-1}\left(\sin\frac{\theta_{inc}}{n}\right) \tag{5}$$

Where n is the index of refraction, $n = 1.00$ for hollow cubes and 1.45 for solid fused silica. The quantity is given by

$$\mu = \sqrt{1 - 2\tan^2\theta_{ref}} \tag{6}$$

Note that this correction factor applies to a single corner cube, but since the satellite backscattering cross-section, σ_{BS}, is proportional to the single corner cube cross-section, σ_{CC}, we apply the correction to the satellite backscattering cross-section. Similar correction terms exist for velocity aberration, when the far-field-diffraction pattern of a cube corner is displaced from the target due to satellite motion. In our analysis, this correction was neglected because we presumed that the spoiling of the corner cube would compensate for velocity aberrations.

Atmospheric Assumptions. The atmospheric effects on retroreflected signal return were estimated through two-way attenuation caused by molecular and aerosol absorption and scattering, and turbulence-induced beam spreading and jitter.

Atmospheric Attenuation. MODTRAN was used to estimate the atmospheric attenuation. We invoked three atmospheric models selectable in MODTRAN: the worst, the nominal, and the best cases. The worst-case model assumed 5-km visibility with subvisible cirrus at 10-km height, 1 km thick. The nominal case presumed 23-km visibility with no aerosols, and the best case presumed a desert extinction model with a wind speed of 12 m/sec. The attenuation at zenith is scaled by the zenith angle using a secant scaling and the loss is squared to account for the round-trip loss.

Atmospheric Turbulence. The Fried parameter, or r_0, is estimated. Again a worst, nominal, and best-case r_0 is invoked from look-up tables that use a Hufnagel–Valley and CLEAR Day models that were used for the Mars Laser Communications Demonstration (MLCD) project. The r_0 values are further scaled by time of day using a boundary layer model.

$$L_{atm\_spread} = \frac{\left[\frac{1}{S} + \left[\frac{1}{\left(1 + (D/r_0)^{\frac{5}{3}}\right)^{\frac{6}{5}}}\right]^{-1} - 1\right]^{-1}}{\exp\left[\frac{1}{S} + \left[\frac{1}{\left(1 + (D/r_0)^{\frac{5}{3}}\right)^{\frac{6}{5}}}\right]^{-1} - 1\right]^{-1}} \tag{7}$$

In Equation (7), S is the Strehl ratio defined earlier; D is the transmitter aperture diameter that was taken as the mean laser spot diameter on the primary mirror.

$$L_{atm\_point} = \frac{\left[\frac{1}{S} + \left[\frac{1}{\left(1 + (D/r_0)^{\frac{5}{3}}\right)^{\frac{6}{5}}}\right]^{-1} + \frac{\sigma_{jitter}}{2\theta_t} - 1\right]^{-1}}{\exp\left[\frac{1}{S} + \left[\frac{1}{\left(1 + (D/r_0)^{\frac{5}{3}}\right)^{\frac{6}{5}}}\right]^{-1} + + \frac{\sigma_{jitter}}{2\theta_t} - 1\right]^{-1}\left[\frac{\theta_{mispoint}}{2\theta_t^2}\right]} \tag{8}$$

Note that σ_{jitter} and $\theta_{mispoint}$ are the radial random and fixed pointing errors of the OCTL mount and were taken to be 5 μrad and 10 μrad to 15 μrad, respectively.

Collection Area. The returned signal irradiance is multiplied by the effective collection area, A, of the OCTL telescope.

Receive Telescope Efficiency. The receive telescope efficiency, η_{Rx_Tel}, accounts for optical reflection losses from all seven OCTL telescope mirrors and transmission through the path-isolation window.

Scatter Efficiency. Due to wavefront error in the receive optics, the loss, or η_{Strehl}, is estimated using $\left[1 - (2\pi\sigma_{WFE})^2\right]$.

Optical Train. The term η_{opt_train} accounts for optical transmission losses through the relay optics in the receiver train.

Polarization Losses. The term η_{POL} accounts for polarization mismatch losses in the return signal path. The maximum polarization loss through the telescope was measured at 6 dB. We estimated minimum and nominal values of 1 dB and 2 dB, respectively. In the results presented, the worst, nominal, and best polarizations and atmospheric conditions were coupled to establish lower and upper bounds on the analysis.

III. Active Satellite Tracking Experiment

OCTL has permission to illuminate in excess of 20 international satellites and has propagated 60-μrad- and 30-μrad-wide beams to target satellites at both 532-nm and 1064-nm wavelengths. Early active satellite tracking experiments to validate telescope pointing used a Q-switched Quanta-Ray LAB190 Nd:YAG laser flash lamp pumped at 50 Hz. A facility instrument, this laser — as are all lasers that use the OCTL for beam propagation — was integrated into the OCTL three-tiered laser safety system [10].

The OCTL laser consisted of two rods in an unstable Gaussian-coupled resonator cavity that allowed efficient energy extraction. The Q-switched emits 600-mJ, 8-ns pulses at the 1064-nm fundamental frequency. At the Type II potassium-titanyl-phosphate (KTP) frequency-doubled output, the laser emits a 250-mJ, 8-ns-long pulse. To avoid pulse collision from more distant targets, the laser is operated at submultiples of the lamp pulse repetition

frequency (PRF). It emits a 7.4-mm by 11.5-mm elliptical beam with divergence of approximately 0.5 milliradian at 532 nm, and 1.9 milliradians at 1064 nm. The Q-switch repetition rate was varied to change the laser pulse emission rate. The flash lamp PRF was maintained at 50 Hz to keep the thermal loading of the cavity constant. With this approach, the beam divergence was maintained constant for the various repetition rates, eliminating the need to realign the optical train for different target satellites. Results showed 3-arcsecond blind pointing of the telescope. Satellites were tracked using files from the International Laser Ranging Service (ILRS) consolidated prediction file (CPF) format. To date, the OCTL has successfully transmitted to EGP-1, Stella, Starlette, and Beacon C, satellites for which CPF files are available [11]. Figure 2(a) shows the uplink from the main telescope; Figure 2(b) shows the Rayleigh backscatter and the Sun-illuminated EGP-1 satellite as seen through the 20-cm acquisition telescope.

(a) (b)

Figure 2. (a) Laser beam transmitted from the main OCTL telescope; (b) Sun-illuminated EGP-1 satellite at the end of the Rayleigh backscattered light.

Returns at 532 nm were detected using the Hamamatsu H5783-20 photomultiplier and the Hamamatsu 9170 near-infrared photomultiplier (see Figure 3) for 1064-nm single photon detection. The 9170 near-infrared photomultiplier tube (PMT) was evacuated and cooled to –60 deg C and set at a bias of approximately –800 V for maximum gain.

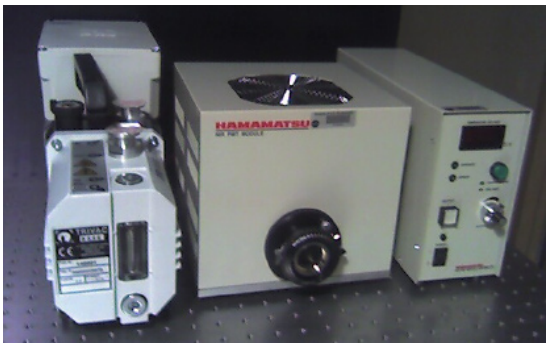

Figure 3. Near-infrared photomultiplier tube with vacuum pump and voltage- and temperature-control electronics.

Both monostatic and bistatic operational modes were used. In monostatic operation, the laser is transmitted through two subapertures on the 1-m primary, and the return is detected through the same aperture. Transmit/receive isolation is achieved via polarization. In bistatic operation, the return signal was detected through a 600-μm core fiber coupled to the 20-cm acquisition telescope boresighted with the 1-m transmitter telescope. This approach isolated the PMT from the 1064-nm radiation scattered in the coudé room. The acquisition telescope is a simple F/7.5 Newtonian telescope, with an annular 20-cm entrance pupil and 1.5-m focal length. A pellicle beamsplitter reflected roughly half of the return signal onto the polished end of the 600-μm diameter, 0.22-NA fiber near the telescope focus, and transmitted the remainder to the acquisition camera. The optical fiber conducted the received signal through the azimuth axis of the telescope to the detector in the coudé room. The fiber output was collimated and filtered through a 10-nm bandpass filter centered at 1064 nm. The monostatic mode was used for the early tracking experiments. Both approaches were used for the Missile Defense Agency (MDA) range-resolved Doppler imaging experiments that were conducted at the OCTL by Boeing/SVS.

The Boeing laser has a 50-W, 1064-nm master oscillator power amplifier system operated with a proprietary macropulse/micropulse format. A weak negative lens at the output of the laser generation and control system was used to generate the appropriate beam divergence entering the telescope. The high beam intensity necessitated testing on a witness sample to ensure that the beam did not damage the FSS-99 protected silver coating of the telescope's final M7 coudé mirror. To keep the heating of the telescope mirror to a minimum (both for protection of the telescope and to minimize thermal beam distortion and wander), the M7 mirror was thoroughly cleaned prior to operation. No damage to the mirror was observed during or after operations.

Validation of telescope pointing and target illumination was achieved by using the OCTL acquisition telescope as a bistatic receive aperture. A bistatic receive system avoided the excessive background generated at 1064 nm from scattering off common optical surfaces, and Rayleigh scattering from the common path of the atmosphere through which the projected and received signal would travel in a monostatic system. It also minimized interference between the OCTL team's tasks of controlling telescope tracking and the target illumination verification, and the Boeing/SVS team's range-resolved Doppler imaging experiments.

A mechanical shutter protected the Hamamatsu 9170-45 PMT from unwanted illumination. The PMT has an internal lens that focuses the incident-collimated light onto the 1.6-mm indium phosphide/indium gallium arsenide phosphide (InP/InGaAsP) photocathode. The detector quantum efficiency is reported to be 0.5 percent at 1064 nm, which was in agreement with our earlier observations. The detector was operated at a high voltage of –800 V in the photon-counting regime. At this voltage, the reported avalanche gain of the detector is 1×10^6, in rough agreement with our observations. Figure 4 shows the output of the H5783-20 linear PMT and that of the H-9170 PMT. As the figure shows, the pulse width is not preserved by the photon-counting PMT. The returns were stored and post-processed to generate a histogram of signal strength versus range.

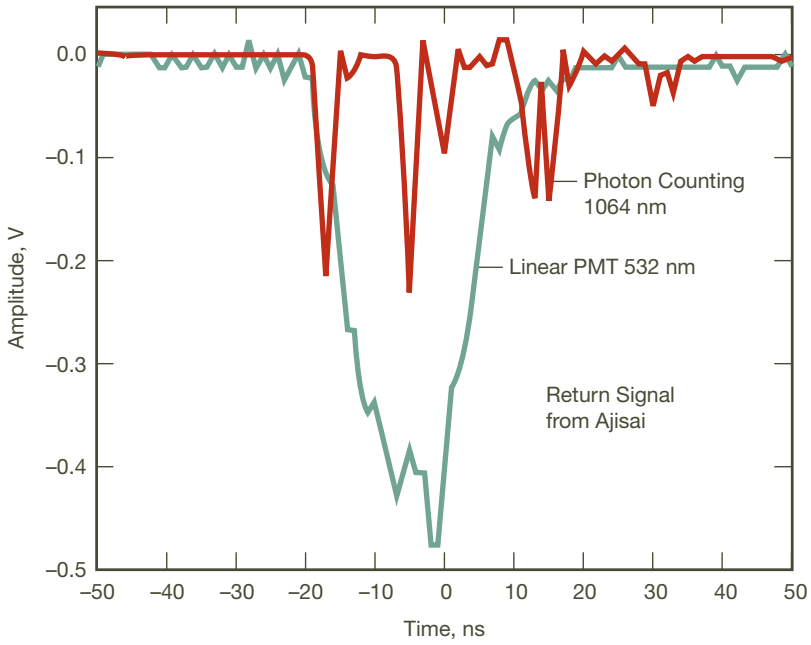

Figure 4. Satellite return signals from Ajisai detected by the H5783-20 linear PMT and by the H-9170 PMT photon counter. The uplink was a 10-ns pulse.

Figure 5 compares theory and experiment for the October 23 Ajisai pass. The uplink beam divergence was 30-μrad full angle. The fit to the data assumed a 3σ pointing error of 15 μrad. There were no clouds visible at the time of the pass, and winds speeds ranged between 1.6 km/hr and 3.2 km/hr. Seeing data were not available at the time of the pass and the large variation in signal return strength during the pass is probably due to fluctuations in beam jitter, tracking errors, and uplink beam scintillation.

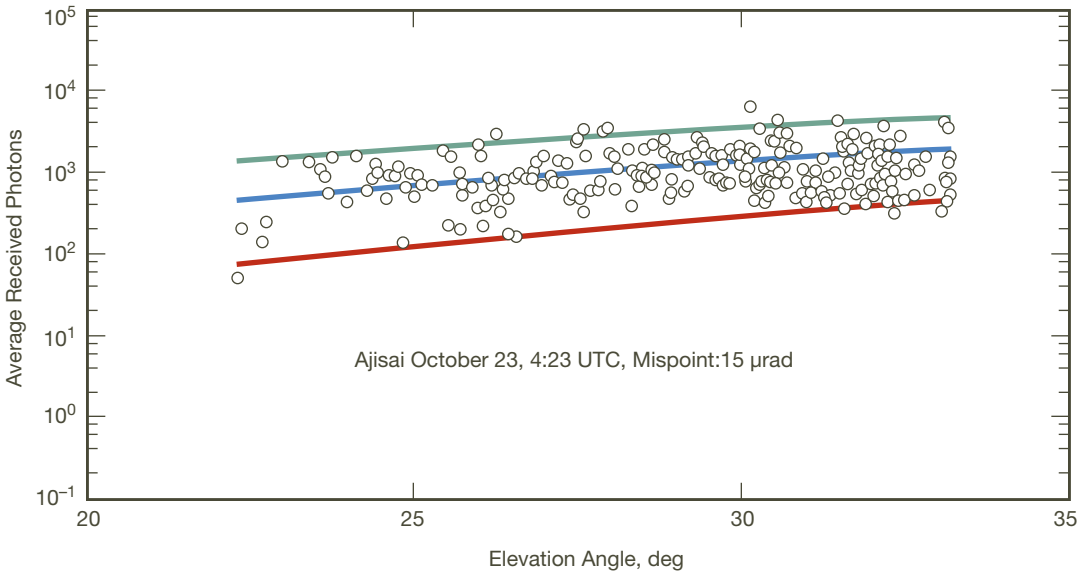

Figure 5. Comparison of predicted (lines) and measured (asterisks) signal returns expressed as number of incident photons versus elevation angle of spacecraft. The 532-nm laser was transmitted from OCTL in the monostatic configuration.

A 10-nm optical filter centered at 1064 nm in the receiver optical train protected the PMT from saturation by the day sky. Figure 6(a) shows the photon count from the early evening sky approximately 30 minutes after sunset. The histogram in Figure 6(b) clearly shows a peak at the expected return from the satellite. A histogram of the return signal from a 22-minute pass of the Beacon C satellite is shown in Figure 7; here, the uplink was the Boeing laser. The 12-km range in the histogram reflects the width of the uplink pulse ~ 40 μsec.

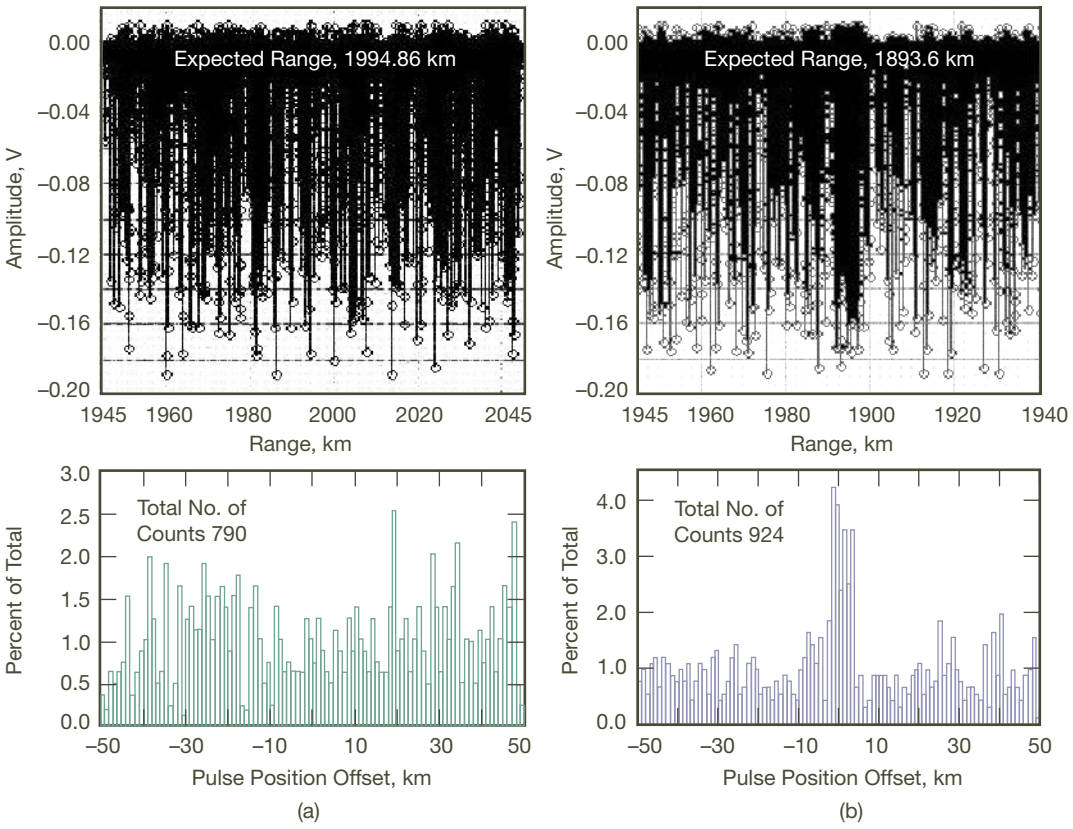

Figure 6. Output of Hamamatsu single-photon detector showing (a) early evening background noise and (b) retroreflected signal return from satellite.

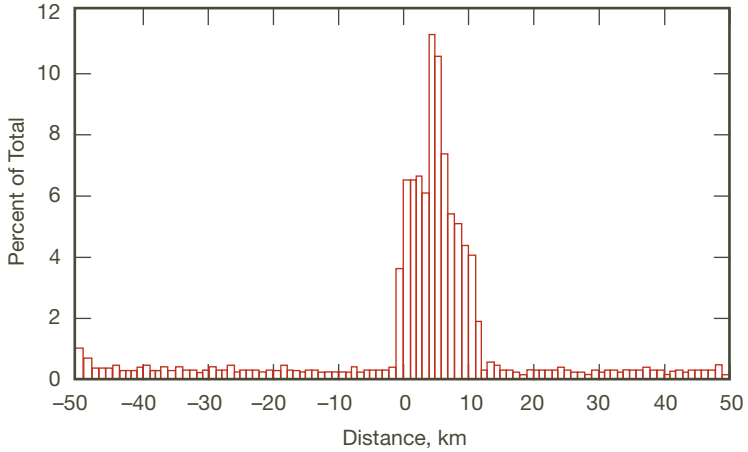

Figure 7. Histogram of all the pulses over a 22-minute run for Beacon C, starting at 3:21:09 UTC on February 11, 2007. The cluster of returns near the expected range is clearly greater than the background.

Acknowledgments

The authors express their appreciation to Lt. Col. Tony Novello of the Missile Defense Agency; J. Ceniceros and his Boeing/SVS and Raytheon team; D. Mayes and A. Grigsby of the Table Mountain Facility; and J. Roberts, M. Troy, and S. Guiwits of JPL.

References

[1] K. E. Wilson and J. R. Lesh, "GOPEX: A Laser Uplink to the Galileo Spacecraft on Its Way to Jupiter," *SPIE Free-Space Laser Communication Technologies Proceedings*, vol. 1866, pp. 138–147, January 1993.

[2] K. E. Wilson, P. R. Leatherman, R. Cleis, J. Spinhirne, and R. Q. Fugate, "Results of the Compensated Earth–Moon–Earth (CEMERELL) Laser Link Experiment," *The Telecommunications and Data Acquisition Progress Report*, vol. 42-131, Jet Propulsion Laboratory, Pasadena, California, pp. 1–13, November 15, 1997. http://tda/progress_report/42-131/131D.pdf

[3] K. Wilson, M. Jeganathan, J. R. Lesh, J. James, and G. Xu, "Results from Phase-1 and Phase-2 GOLD Experiments," *The Telecommunications and Data Acquisition Progress Report*, vol. 42-128, Jet Propulsion Laboratory, Pasadena, California, pp. 1–11, February 15, 1997. http://tda/progress_report/42-128/128K.pdf

[4] A. Alonso, M. Reyes, and Z. Sodnik, "Performance of Satellite-to-Ground Communications Link Between ARTEMIS and the Optical Ground Station," *SPIE Optics in Atmospheric Propagation and Adaptive Systems VII Proceedings*, vol. 5572, November 2004.

[5] M. Toyoshima, T. Takahashi, K. Suzuki, S. Kimura, K. Takizawa, T. Kuri, W. Klaus, M. Toyoda, H. Kunimori, T. Jono, Y. Takayama, and K. Arai, "Laser Beam Propagation in Ground-to-OICETS Laser Communication Experiments," *SPIE Atmospheric Propagation IV Proceedings*, vol. 6551, May 2007.

[6] T. Jono, Y. Takayama, K. Shiratama, I. Mase, B. Demelenne, Z. Sodnik, A. Bird, M. Toyoshima, H. Kunimori, D. Giggenbach, N. Perlot, M. Knapek, and K. Arai, "Overview of the Inter-Orbit and the Orbit-to-Ground Laser Communication Demonstration by OICETS," *SPIE Free-Space Laser Communication Technologies XIX and Atmospheric Propagation of Electromagnetic Waves*, vol. 6457, February 2007.

[7] A. H. Vaughan and D. Mayes, "Optical Metrology of the Optical Communications Telescope Laboratory 1-Meter Telescope by Means of Hartmann Tests Conducted at the Table Mountain Observatory," *The Interplanetary Network Progress Report*, vol. 42-161, Jet Propulsion Laboratory, Pasadena, California, pp. 1–14, May 15, 2005. http://tda/progress_report/42-161/161C.pdf

[8] A. E. Siegman, "The Antenna Properties of Optical Heterodyne Receivers," *Proceedings of the IEEE*, vol. 54, no. 10, pp. 1350–1356, October 1966.

[9] http://www.wettzell.ifag.de/publ-cgi-bin/linkbudget.py

[10] K. E. Wilson, F. W. Battle, and B. Smithgall, "Laser Operations at JPL/NASA OCTL Facility," International Laser Safety Conference, San Francisco, California, March 19–22, 2007.

[11] R. L. Ricklefs, "Consolidated Laser Ranging Prediction Format, Version 1.01," February 2006. ftp://cddis.gsfc.nasa.gov/pub/slr/cpf_predicts